Synthesis, structures and thermal decomposition of ammine $M_xB_{12}H_{12}$ complexes (M = Li, Na, Ca)

Hansen, Bjarne R.S.; Tumanov, Nikolay; Santoru, Antonio; Pistidda, Claudio; Bednarcik, Jozef; Klassen, Thomas; Dornheim, Martin; Filinchuk, Yaroslav; Jensen, Torben R.

Published in:
Dalton Transactions

DOI:
10.1039/c7dt01414g

Publication date:
2017

Dalton Transactions

PAPER

View Article Online
View Journal | View Issue

Cite this: *Dalton Trans.*, 2017, **46**, 7770

Synthesis, structures and thermal decomposition of ammine $M_xB_{12}H_{12}$ complexes (M = Li, Na, Ca)†

Bjarne R. S. Hansen,[a] Nikolay Tumanov,[b,c] Antonio Santoru,[d] Claudio Pistidda,[d] Jozef Bednarcik,[e] Thomas Klassen,[d] Martin Dornheim,[d] Yaroslav Filinchuk[b] and Torben R. Jensen*[a]

A series of ammine metal-dodecahydro-*closo*-dodecaboranes, $M_xB_{12}H_{12}{\cdot}nNH_3$ (M = Li, Na, Ca) were synthesized and their structural and thermal properties studied with *in situ* time-resolved synchrotron radiation powder X-ray diffraction, thermal analysis, Fourier transformed infrared spectroscopy, and temperature-programmed photographic analysis. The synthesized compounds, $Li_2B_{12}H_{12}{\cdot}7NH_3$, $Na_2B_{12}H_{12}{\cdot}4NH_3$ and $CaB_{12}H_{12}{\cdot}6NH_3$, contain high amounts of NH_3, 43.3, 26.6 and 35.9 wt% NH_3, respectively, which can be released and absorbed reversibly at moderate conditions without decomposition, thereby making the *closo*-boranes favorable 'host' materials for ammonia or indirect hydrogen storage in the solid state. In this work, fifteen new ammine metal dodecahydro-*closo*-dodecaborane compounds are observed by powder X-ray diffraction, of which six are structurally characterized, $Li_2B_{12}H_{12}{\cdot}4NH_3$, $Li_2B_{12}H_{12}{\cdot}2NH_3$, $Na_2B_{12}H_{12}{\cdot}4NH_3$, $Na_2B_{12}H_{12}{\cdot}2NH_3$, $CaB_{12}H_{12}{\cdot}4NH_3$ and $CaB_{12}H_{12}{\cdot}3NH_3$. $Li_2B_{12}H_{12}{\cdot}4NH_3$ and $Na_2B_{12}H_{12}{\cdot}4NH_3$ are isostructural and monoclinic ($P2_1/n$) whereas $Na_2B_{12}H_{12}{\cdot}2NH_3$ and $CaB_{12}H_{12}{\cdot}3NH_3$ are both trigonal with space groups $P\bar{3}m1$ and $R\bar{3}c$, respectively. Generally, coordination between the metal and the icosahedral *closo*-borane anion is diverse and includes point sharing, edge sharing, or face sharing, while coordination of ammonia always occurs *via* the lone pair on nitrogen to the metal. Furthermore, a liquid intermediate is observed during heating of $Li_2B_{12}H_{12}{\cdot}7NH_3$. This work provides deeper insight into the structural, physical, and chemical properties related to thermal decomposition and possible ammonia and hydrogen storage.

Received 19th April 2017,
Accepted 29th May 2017

DOI: 10.1039/c7dt01414g

rsc.li/dalton

Introduction

Metal borohydrides have received significant scientific attention, owing to their potential use for hydrogen storage.[1–4] However, light metal borohydrides generally decompose at high temperatures due to unfavorable thermodynamic and kinetic properties. Furthermore, reversible hydrogen storage is challenging to achieve owing to formation of stable metal dodecahydro-*closo*-dodecaboranes, $M_xB_{12}H_{12}$,[5] during decomposition, which hampers hydrogen release and uptake.[6–11] However, metal dodecahydro-*closo*-dodecaboranes are a versatile class of compounds, which may have potential use in cancer treatment,[12,13] as ion conductors,[14–17] in polymer chemistry,[18] hydrogen storage,[19] or ammonia storage materials (indirect hydrogen storage).[5,20] Recently, attention has been directed towards ammonia, NH_3, as a hydrogen carrier.[21] Although the storage of liquid ammonia in a steel vessel is well established, solid-state storage can mitigate the hazards of toxicity and smell, while retaining a high hydrogen density.[22] NH_3 contains 17.7 wt% H, and can coordinate to metal cations to form solid ammine complexes, *i.e.* $MgCl_2{\cdot}6NH_3$, $Mn(BH_4)_2{\cdot}6NH_3$, $Li_2B_{12}H_{12}{\cdot}7NH_3$, or $Rb_2B_{10}H_{10}{\cdot}5NH_3$.[20,23–25] These compounds can be considered potential candidates for solid-state ammonia storage. In low-temperature polymer electrolyte membrane fuel cell (LT PEM FC) applications, the use of NH_3(g) can be detrimental, but NH_3 can be split into H_2 and N_2 using an appropriate catalyst

[a]*Center for Materials Crystallography, iNANO, and Department of Chemistry, Aarhus University, Langelandsgade 140, 8000 Aarhus, Denmark. E-mail: trj@chem.au.dk*
[b]*Institute of Condensed Matter and Nanosciences, Université catholique de Louvain, Place L. Pasteur 1, 1348 Louvain-la-Neuve, Belgium*
[c]*Chemistry Department, Université de Namur, Rue de Bruxelles 61, 5000 Namur, Belgium*
[d]*Institute of Materials Research, Nanotechnology, Helmholtz-Zentrum Geesthacht GmbH, Max-Planck-Strasse 1, D-21502 Geesthacht, Schleswig-Holstein, Germany*
[e]*Deutsches Elektronen-Synchrotron (DESY), Notkestrasse 85, Hamburg, 22607, Germany*

†Electronic supplementary information (ESI) available. CCDC 1489211 ($CaB_{12}H_{12}{\cdot}3NH_3$), 1489212 ($Li_2B_{12}H_{12}{\cdot}4NH_3$), 1489213 ($Na_2B_{12}H_{12}{\cdot}2NH_3$) and 1489214 ($Na_2B_{12}H_{12}{\cdot}4NH_3$). For ESI and crystallographic data in CIF or other electronic format see DOI: 10.1039/c7dt01414g

(typically Ni or Ru)[23] or using $NaNH_2$-mediated NH_3 cracking.[26,27] Ammonia can also be used directly in a solid oxide fuel cell (SOFC) with a Fe-based catalyst.[28] Additionally, ammonia can be used in reduction of NO_x exhaust gasses in diesel vehicles, *e.g.* with NH_3 stored in a solid metal halide salt.[29–32] Previously, formation of $Li_2B_{12}H_{12}{\cdot}7NH_3$ has been demonstrated from $Li_2B_{12}H_{12}$ in contact with gaseous or liquid NH_3,[20] and $Rb_2B_{12}H_{12}{\cdot}8NH_3$, $Cs_2B_{12}H_{12}{\cdot}6NH_3$ and $Rb_2B_{10}H_{10}{\cdot}5NH_3$ have been structurally investigated, but are only stable at $T < -38$ °C.[25]

In the following, the NH_3 uptake and release properties of a series of ammine metal-dodecahydro-*closo*-dodecaboranes are described. $Li_2B_{12}H_{12}{\cdot}7NH_3$, $Na_2B_{12}H_{12}{\cdot}4NH_3$ and $CaB_{12}H_{12}{\cdot}6NH_3$ are synthesized and studied with *in situ* time-resolved synchrotron radiation powder X-ray diffraction (*in situ* SR-PXD), thermal analysis (TGA-DSC-MS), Fourier transformed infrared spectroscopy (FTIR) and temperature-programmed photographic analysis (TPPA), revealing up to fifteen new compounds, where six are structurally determined.

Experimental

Sample preparation

Metal dodecahydro-*closo*-dodecaboranes, $M_xB_{12}H_{12}$ (M = Li, Na and Ca) were purchased from Katchem, Prague, Czech Republic. Anhydrous materials were obtained by heating the as-received samples to 230 °C under dynamic vacuum for 10 hours, following an earlier reported procedure.[33] The anhydrous $M_xB_{12}H_{12}$ (M = Li, Na and Ca) compounds were placed in a round bottom flask under Ar atmosphere, which was cooled by a water bath ($T \approx$ 5–10 °C). A flow of NH_3 was passed over the sample for *ca.* 15 minutes, without air exposure. Shortly after start of NH_3 flow (30 to 120 seconds), the volume of the powders increased and the reaction was exothermic (an initial synthesis, without a cooling bath, revealed the flask was hot to the touch). Table 1 presents an overview of the samples. It should be noted that $K_2B_{12}H_{12}$ does not react with NH_3 at the applied conditions (see ESI†).

Reversible NH_3 release and uptake in $Na_2B_{12}H_{12}{\cdot}4NH_3$ and $CaB_{12}H_{12}{\cdot}6NH_3$ was studied by heating the samples under dynamic vacuum to either 250 or 300 °C ($\Delta T/\Delta t$ = 10 °C min^{-1}), kept isothermally for 30 minutes and then cooled naturally to RT. The samples were then placed in the flask again and exposed to a flow of gaseous NH_3 as described above. Diffractograms were obtained at RT after each step (Fig. 13 and 14).

Table 1 Sample overview of $M_xB_{12}H_{12}$ and $M_xB_{12}H_{12}{\cdot}nNH_3$ (M = Li, Na, Ca). The synthesis was performed by passing a flow of gaseous NH_3 through the sample at $T \approx$ 5–10 °C

Reactants	Product
$Li_2B_{12}H_{12}{\cdot}4H_2O$ heated to 230 °C for 10 h, dyn. vac.	$Li_2B_{12}H_{12}$
$Li_2B_{12}H_{12}$ + NH_3 (g)	$Li_2B_{12}H_{12}{\cdot}7NH_3$
$Na_2B_{12}H_{12}{\cdot}xH_2O$ heated to 230 °C for 10 h, dyn. vac.	$Na_2B_{12}H_{12}$
$Na_2B_{12}H_{12}$ + NH_3 (g)	$Na_2B_{12}H_{12}{\cdot}4NH_3$
$CaB_{12}H_{12}{\cdot}H_2O$ heated to 230 °C for 10 h, dyn. vac.	$CaB_{12}H_{12}$
$CaB_{12}H_{12}$ + NH_3 (g)	$CaB_{12}H_{12}{\cdot}6NH_3$

Thermal analysis

Thermogravimetric analysis (TGA) and differential scanning calorimetry (DSC) was performed on a Netzsch STA 409 C, which was connected *via* a capillary tube (*ca.* 2 m) to a Hiden Analytical HAL 201 mass spectrometer (MS). The samples were transferred to Al_2O_3 crucibles under argon atmosphere in a glove box with circulation purifier ($p(O_2, H_2O)$ < 1 ppm) and heated from RT–585 °C ($\Delta T/\Delta t$ = 5 °C min^{-1}) in the combined system under an Ar-flow of 50 mL min^{-1}.

Fourier transformed infrared spectroscopy (FTIR)

Attenuated Total Reflectance Fourier Transformed Infrared spectroscopy was conducted in a Nicolet 380 Avatar spectrometer. The sample was placed over the infrared radiation source and immediately covered by a tight screw. Thus, the total air exposure of the materials is limited to a few seconds. The spectra were collected in the wavenumber range of 4000–400 cm^{-1} with 32 scans and wavenumber resolution of 4 cm^{-1} (data spacing 1.929 cm^{-1}).

In-house powder X-ray diffraction (PXD)

In-house PXD was carried out using a Bruker D8 Discover X-ray diffractometer with Cu radiation (Cu Kα, 50 kV, 40 mA) and VANTEC-500 2D detector. Air-tight sample holders (Bruker, Germany) were used to prevent contamination of the sample. Otherwise PXD was performed using a Rigaku Smart Lab X-ray diffractometer configured with a Cu X-ray source and a parallel beam multilayer mirror (Cu Kα, λ = 1.5418 Å). Data were collected at RT between 5° and 55° 2θ at 2° min^{-1}. Samples were mounted in 0.5 mm borosilicate glass capillaries and sealed with glue.

Synchrotron radiation powder X-ray diffraction (SR-PXD)

In situ time-resolved SR-PXD data were measured at beamline X04SA at the Swiss Light Source (SLS), Villigen, Switzerland, at beamline I711 at the synchrotron MAX-II, Lund, Sweden, or at beamline P02.1 at Petra III, Deutsches Elektronen Synchrotron (DESY), Hamburg, Germany.

At SLS, the SR-PXD data were collected with a MYTHEN detector at a wavelength of 0.7750 Å. A standard LaB_6 sample was used for calibration. All samples were sealed in 0.5 mm glass capillaries (wall thickness 0.01 mm) under helium atmosphere and were measured at variable temperature using a heating rate of $\Delta T/\Delta t$ = 5° min^{-1}.

At MAXlab, SR-PXD data were collected with a MAR165 CCD detector system and a wavelength of 0.9938 Å.[34] The used sample cell was specially developed for studies of gas/solid reactions and allows variable pressures and temperatures to be applied.[35–37] The powdered samples were mounted in a sapphire single-crystal tube (Al_2O_3, outer diameter 1.09 mm, inner diameter 0.79 mm), inside an argon-filled glove box ($p(O_2, H_2O)$ < 1 ppm). The sample temperature was controlled with a hot air blower temperature-calibrated to an internal NaCl

sample. During desorption measurements the samples were typically heated to 450 °C with a heating rate of $\Delta T/\Delta t$ = 5 °C min^{-1} under ~1 bar Ar.

At Petra III, the formation of ammine metal dodecahydro-*closo*-boranes was studied by loading the anhydrous samples in sapphire single-crystal tube (Al_2O_3, outer diameter 1.0 mm, inner diameter 0.6 mm) and measured at RT with varying ammonia pressure, 0 < $p(NH_3)$ < 6.5 bar, at beamline P02.1 (DESY), which is equipped with an amorphous silicon area detector (PerkinElmer XRD1621) and a wavelength of λ = 0.2077 Å.[38] The experiments were performed according to a previous report.[39]

The FIT2D program was used to remove diffraction spots originating from the single-crystal sapphire tubes and subsequently to transform raw data to powder patterns.[40]

Crystal structure determination

Data collected at the Materials Science Beamline at SLS (PSI) were used for structure solution and refinement. Powder patterns were indexed using the FOX software.[41] Structures were solved by direct-space Monte Carlo methods using FOX[41] and were refined using Rietveld method by Fullprof Suite software.[42] Details of structure determination for each compound are given in ESI.† Final Rietveld refinements plots and refinement indicators are shown in Fig. S5–S8,† and experimental structural parameters and atomic coordinates are listed in Tables S2–S9.†

Temperature-programmed photographic analysis (TPPA)

Temperature-programmed photographic analysis was performed by collecting photographs using a digital camera while heating the samples from RT to 350 or 400 °C ($\Delta T/\Delta t$ = 5 °C min^{-1}) using a setup previously described.[43] Samples (~15 mg) were pressed into pellets (5 mm diameter) and sealed under argon in a glass vial connected to an argon-filled balloon to maintain an inert atmosphere and constant pressure. A thermocouple was in contact with the sample within the glass vial to monitor the temperature during thermolysis. The glass vial was encased within an aluminum block with open viewing windows for photography, to provide near-uniform heating by cartridge heaters, interfaced to a temperature controller.

Results

Initial sample characterization

All metal dodecahydro-*closo*-dodecaborane samples were characterized with FTIR and PXD before and after ammonia-treatment, as shown in Fig. 1 and 2. Vibrational signals for the $[B_{12}H_{12}]^{2-}$-anion are observed in all samples at *ca.* 2480, 1070 and 720 cm^{-1} in accord with previous work[44] or predicted by DFT calculations.[45,46] This shows that the $B_{12}H_{12}$-icosahedra are still present after the ammonia treatment, underlining the chemical stability of the metal dodecahydro-*closo*-dodecaboranes. Note, however, that the B–H stretching peaks

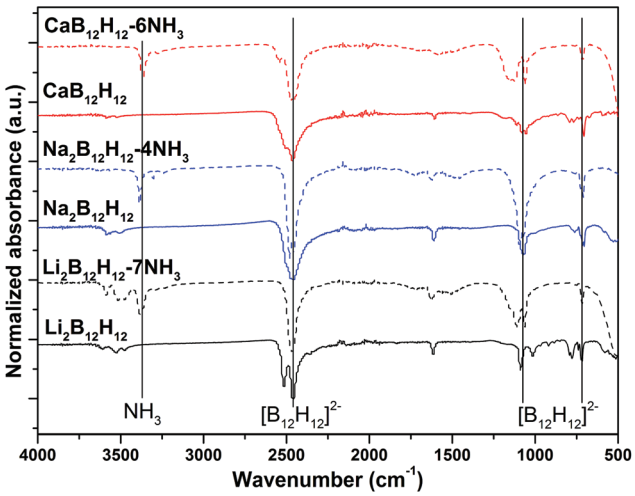

Fig. 1 FTIR spectra of the $M_xB_{12}H_{12}$ samples (M = Li, Na, Ca) before (solid line) and after NH_3 flow treatment (dashed line).

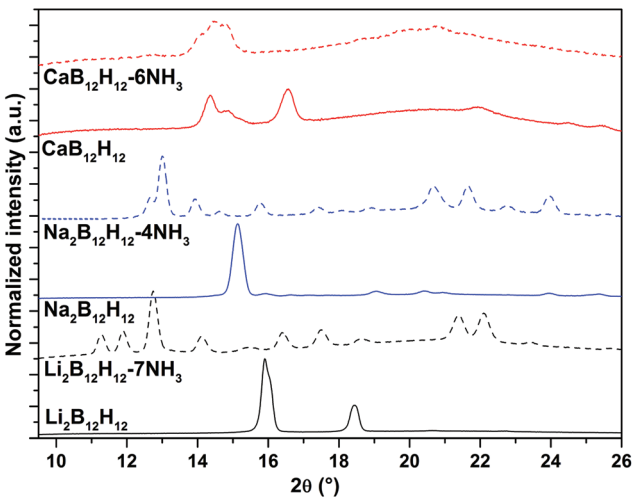

Fig. 2 Powder X-ray diffractograms of the $M_xB_{12}H_{12}$ samples (M = Li, Na, Ca) before (solid line) and after NH_3 flow treatment (dashed line), λ = 1.5418 Å. Data were obtained at RT in all cases.

(~2480 cm^{-1}) merge into one peak after NH_3 treatment. This has previously been observed and is attributed to a gain in symmetry of the boron icosahedra.[20,47] Vibrational signals from NH_3 are observed at 3380 cm^{-1} (N–H stretch) and 1140 cm^{-1} (N–H wagging) in the ammine metal dodecahydro-*closo*-dodecaborane samples. Minor O–H stretching and bending modes from H_2O are also observed in the samples despite being in a dehydrated state, likely because the samples were briefly exposed to air, and metal dodecahydro-*closo*-dodecaboranes are known to be deliquescent.[19]

Diffractograms of the reactant $M_xB_{12}H_{12}$ (M = Li, Na, Ca) are consistent with the known structures of anhydrous $Li_2B_{12}H_{12}$, $Na_2B_{12}H_{12}$ and $CaB_{12}H_{12}$, whereas diffractograms of the ammoniated samples reveal unknown diffraction patterns

(Fig. 2). The ammine lithium dodecahydro-*closo*-dodecaborane sample is identical to the previously reported $Li_2B_{12}H_{12}{\cdot}7NH_3$, which was synthesized in a similar way,[20] and from structure solutions using the *in situ* SR-PXD at SLS, $Na_2B_{12}H_{12}{\cdot}4NH_3$ was determined (discussed later). Rietveld refinement of the RT diffractogram from the *in situ* SR-PXD confirms the presence of $Li_2B_{12}H_{12}{\cdot}7NH_3$ using the reported structural model of $Li_2B_{12}H_{12}{\cdot}7NH_3$ extracted from single-crystal diffraction (Fig. S4†). However, the powdered sample of $Li_2B_{12}H_{12}{\cdot}7NH_3$ reveals diffraction peaks at 2θ = 8.90° (1 1 2) and 9.02° (0 1 3) not observed in the previously reported experimental data and a broad Bragg peak at 2θ = 7.78° (−1 1 2) not included in the calculated model.[20] The broad peak at 2θ = 7.78° may be due to stacking faults generated by the *n*-glide plane.

The *in situ* formation of ammine metal dodecahydro-*closo*-dodecaboranes was also studied at synchrotron facility Petra III, using a setup described elsewhere.[39] The data clearly indicate a complete one-step ammonia uptake reaction within ~30 seconds of exposure to gaseous NH_3 (Fig. S1–S3†). The composition of two products obtained after the reaction with ammonia was derived by structural solution to be $Li_2B_{12}H_{12}{\cdot}7NH_3$ and $Na_2B_{12}H_{12}{\cdot}4NH_3$ and the composition of the calcium compound is estimated to $CaB_{12}H_{12}{\cdot}6NH_3$ based on the thermal analysis; however structure solution was not possible.

Structural analysis of the series $M_xB_{12}H_{12}$ (M = Li, Na, Ca)

Six new ammine metal dodecahydro-*closo*-borane compounds are identified and structurally investigated using *in situ* time resolved SR-PXD data and the crystallographic details are listed in Table 2 and atomic coordinates and bond lengths are provided in Tables S2–S9 in the ESI.†

The known compound $Li_2B_{12}H_{12}{\cdot}7NH_3$, decomposes *via* two intermediates; $Li_2B_{12}H_{12}{\cdot}4NH_3$ (observed in the temperature range 60 to 200 °C) and $Li_2B_{12}H_{12}{\cdot}2NH_3$ (observed in the temperature range 190 to 210 °C). In the latter case, PXD data quality did not allow complete structural solution, but a chemical composition is proposed in a cubic unit cell, a = 20.8754(3) Å and space group $I2_13$ (Table 2).

The structure of $Li_2B_{12}H_{12}{\cdot}4NH_3$ ($P2_1/n$) is shown in Fig. 3, where Li-atoms coordinate to two $[B_{12}H_{12}]^{2-}$ anions *via* a single H-atom (point sharing, η^1) or three H-atoms (face sharing, η^3), respectively (Li–H distances vary between 1.87 (η^1) to 2.24 Å (η^3)). Each Li-atom coordinates to two NH_3 molecules *via* the lone pair on nitrogen and Li–N bond distances are in the range 2.31 to 2.46 Å. In total, Li-atoms coordinate to two NH_3 molecules and four H-atoms, generating distorted octahedra around Li.

The directly synthesized ammine sodium dodecahydro-*closo*-dodecaborane, $Na_2B_{12}H_{12}{\cdot}4NH_3$, is isostructural to $Li_2B_{12}H_{12}{\cdot}4NH_3$ but with a larger unit cell. Rietveld refinement of the structural model is shown in Fig. S7.†

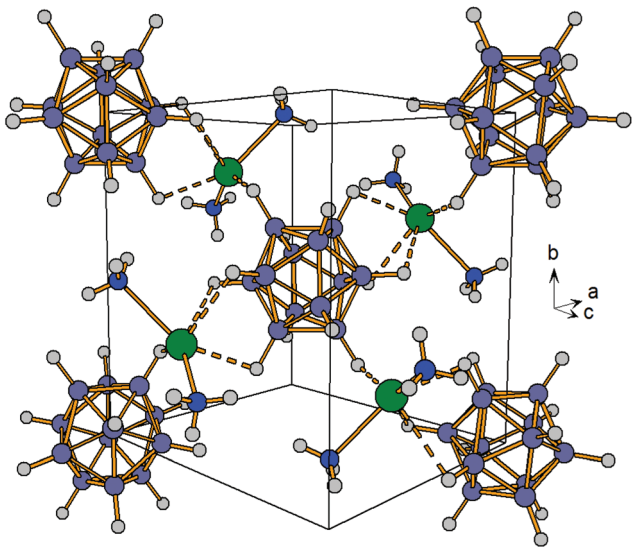

Fig. 3 The crystal structure of $Li_2B_{12}H_{12}{\cdot}4NH_3$ ($P2_1/n$) where Li-atoms coordinate to four H-atoms (dashed) and two NH_3-molecules, generating a distorted octahedra around the Li-atoms. Hydrogen positions are tentative. Atoms are shown as colored spheres: Li (olive), N (blue), B (blue-grey) and H (grey). More structural information is available in Table 2 and Table S2, S3.†

Table 2 Structural data and hydrogen content for the new ammine metal dodecahydro-*closo*-dodecaboranes, $M_xB_{12}H_{12}{\cdot}nNH_3$ (M = Li, Na, Ca)

Chemical Formula	$Li_2B_{12}H_{12}{\cdot}4NH_3$	$Li_2B_{12}H_{12}{\cdot}2NH_3$ [b]	$Na_2B_{12}H_{12}{\cdot}4NH_3$	$Na_2B_{12}H_{12}{\cdot}2NH_3$	$CaB_{12}H_{12}{\cdot}4NH_3$ [b]	$CaB_{12}H_{12}{\cdot}3NH_3$
Crystal system	Monoclinic	Cubic	Monoclinic	Trigonal	Monoclinic	Trigonal
Space group	$P2_1/n$ (no. 14)	$I2_13$ (no. 199)	$P2_1/n$ (no. 14)	$P\bar{3}m1$ (no. 164)	—	$R\bar{3}c$ (no. 167)
T[a] [°C]	100	200	RT	120	100	225
a [Å]	8.4122(3)	20.8754(3)	8.6875(2)	7.1672(1)	11.964(2)	11.8695(2)
b [Å]	9.5193(5)	20.8754(3)	9.4168(3)	7.1672(1)	8.5635(13)	11.8695(2)
c [Å]	9.6434(5)	20.8754(3)	9.9096(3)	7.1574(2)	14.498(2)	16.7978(5)
β [°]	99.472(4)	90	98.3296(18)	90	93.752(6)	90
V [Å^3]	761.70(7)	9097.13(20)	802.14(4)	318.41(1)	1482.2(4)	2049.40(8)
Z	2	32	2	1	4	6
M [g mol^{-1}]	223.83	189.83	255.93	221.87	250.00	233.00
ρ(calc) [g mL^{-1}]	0.98	1.12	1.06	1.16	1.12	1.13
ρ_m (H_2) [wt%]	10.83	9.57	9.47	8.19	9.69	9.10
ρ_V (H_2) [kg H_2 per m^3]	105.66	106.17	100.34	94.79	108.60	103.09
CCDC number	1489212	—	1489214	1489213	—	1489211

[a] Temperature for data collection. [b] Proposed composition.

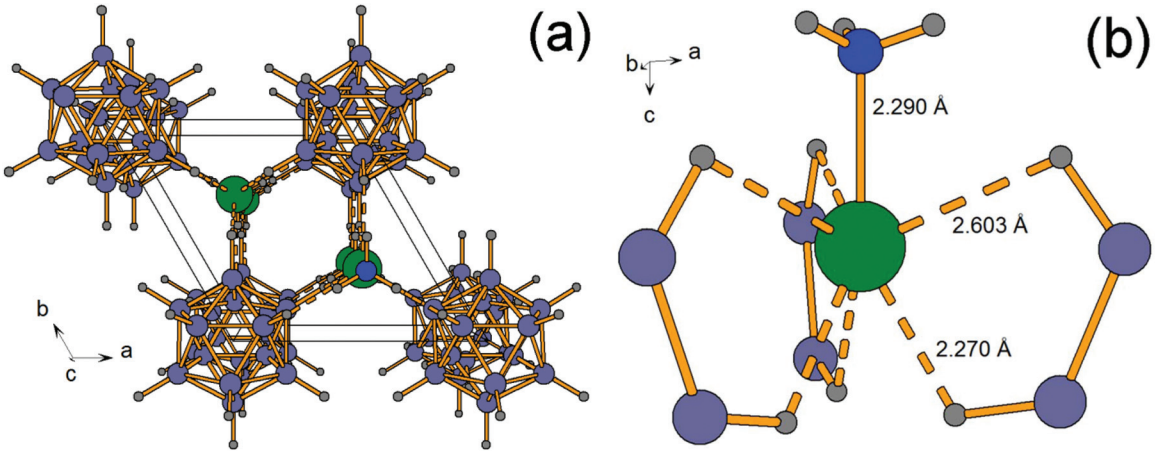

Fig. 4 The crystal structure of $Na_2B_{12}H_{12}{\cdot}2NH_3$ ($P\bar{3}m1$) showing (a) the unit cell and (b) coordination sphere of Na-atoms. Na-Atoms (CN = 7) coordinate to six H-atoms (dashed) and one NH_3-molecule. Bond distances for coordinating atoms are shown. Atoms are shown as colored spheres: Na (olive), N (blue), B (blue-grey) and H (grey). More structural information is available in Table 2 and Table S6, S7.†

An intermediate ammine sodium dodecahydro-*closo*-dodecaborane compound is observed by *in situ* SR-PXD in the temperature range 65 to 120 °C. The composition was determined as $Na_2B_{12}H_{12}{\cdot}2NH_3$, which crystallizes in the trigonal space group $F\bar{3}m1$, a = 7.1672(1) Å, c = 7.1574(2) Å, see Fig. 4. The $[B_{12}H_{12}]^{2-}$-anions are located at the corners of the unit cell, and Na-atoms are surrounded by three $[B_{12}H_{12}]^{2-}$-anions (coordinated *via* edge sharing, η^2) and one NH_3 molecule (directed along the *c*-axis) in a tetrahedral manner, even though the coordination number, CN(Na) = 7 (Fig. 4b). The Na–H bond distance is 2.27 Å and the Na–N distance is 2.29 Å, which is slightly shorter than in $Na_2B_{12}H_{12}{\cdot}4NH_3$ (Na–N distances in the range 2.40 to 2.43 Å).

The initial structure and chemical composition of the synthesized ammine calcium dodecahydro-*closo*-dodecaborane cannot be determined from X-ray data, owing to overlapping Bragg peaks and relatively low crystallinity. However, thermal analysis suggests the composition $CaB_{12}H_{12}{\cdot}6NH_3$ (discussed later). In the *in situ* SR-PXD experiment, two intermediate compounds are structurally identified as $CaB_{12}H_{12}{\cdot}4NH_3$, observed in the temperature range 90 to 190 °C and $CaB_{12}H_{12}{\cdot}3NH_3$ from 190 to 260 °C. The SR-PXD data quality did not allow complete structural solution of $CaB_{12}H_{12}{\cdot}4NH_3$ but a monoclinic unit cell was indexed (Table 2).

In the structure of $CaB_{12}H_{12}{\cdot}3NH_3$, shown in Fig. 5, Ca-atoms have 9-fold coordination; six H-atoms in total, as each $[B_{12}H_{12}]^{2-}$-anion coordinates to the Ca-atom by tridentate face sharing (η^3), and three NH_3 molecules that coordinate equatorially. Thus, the geometry is a tricapped trigonal prism, which is typical for CN = 9. The H-positions are tentative and on NH_3 the hydrogen atoms are disordered by a two-fold axis. Hence, six H positions with occupancy 0.5 are shown, because of temperature disorder. The Ca–N distance is 2.46 Å, which is in line with the Ca–N distance in $CaCl_2{\cdot}8NH_3$ (2.52 Å)[48] and the Ca–H (from $B_{12}H_{12}$) distance is 2.59 Å. The structure stacks along the *c*-axis as observed in Fig. 5b, forming one-dimensional chains. $CaB_{12}H_{12}{\cdot}3NH_3$ is isostructural to $CaB_{12}H_{12}{\cdot}3H_2O$, where the Ca–O distance is 2.33 Å.[49]

In Fig. 6 the unit cell volume per formula unit (V/Z) of the known and new ammine metal dodecahydro-*closo*-dodecaborane compounds is plotted *versus* the number of NH_3 molecules in the structure. Linear fits of $Li_2B_{12}H_{12}{\cdot}n NH_3$, $Na_2B_{12}H_{12}{\cdot}n NH_3$ and $CaB_{12}H_{12}{\cdot}n NH_3$ volumes per formula unit (V/Z) show slopes of 37.3 Å^3/NH_3 (R^2 = 0.9964), 34.9 Å^3/NH_3 (R^2 = 0.9953) and 34.8 Å^3/NH_3 (R^2 = 0.9991), which reflects the size of one NH_3 molecule. This agrees well with the volume of NH_3 in the solid state $V(NH_3)$ = 33.9 Å^3, at T = −80 °C,[50] and follows the same trend as observed for other ammine metal borohydrides reported previously, $M(BH_4)_x{\cdot}n NH_3$ (M = Sr, Ca,[51] Y, Gd, Dy[52] and Mn[24]). Notice, not all data are measured at RT, which may give rise to increased volumes, owing to thermal expansion, and thus larger slopes on Fig. 6.

The ability of a metal dodecahydro-*closo*-dodecaborane to coordinate NH_3 is related to the charge density of the cation, but also the size of the anion. Hence, $Li_2B_{12}H_{12}$ can coordinate seven NH_3, $Na_2B_{12}H_{12}$ coordinates four NH_3, whereas $K_2B_{12}H_{12}$ does not coordinate any NH_3 in structures stable at RT. Furthermore, $Na_2B_{12}H_{12}$ coordinates four NH_3, whereas $NaBH_4$ does not react with NH_3.[1] Thus it seems that higher cation charge density and large, weakly coordinating anions may provide higher amounts of ammonia in the solid state. In addition, more NH_3 can be stored in these compounds by lowering temperature during synthesis, *i.e.* $[Li(NH_3)_4]_2B_{12}H_{12}{\cdot}2NH_3$ was formed at −78 °C, but transforms into $Li_2B_{12}H_{12}{\cdot}7NH_3$ at RT.[25]

Thermal decomposition of ammine metal dodecahydro-*closo*-dodecaboranes

Thermal decomposition of $Li_2B_{12}H_{12}{\cdot}7NH_3$. To elucidate the decomposition mechanism of $Li_2B_{12}H_{12}{\cdot}7NH_3$, *in situ* SR-PXD (Fig. 7), TGA-DSC-MS (Fig. 8), and TPPA (Fig. S9†) was per-

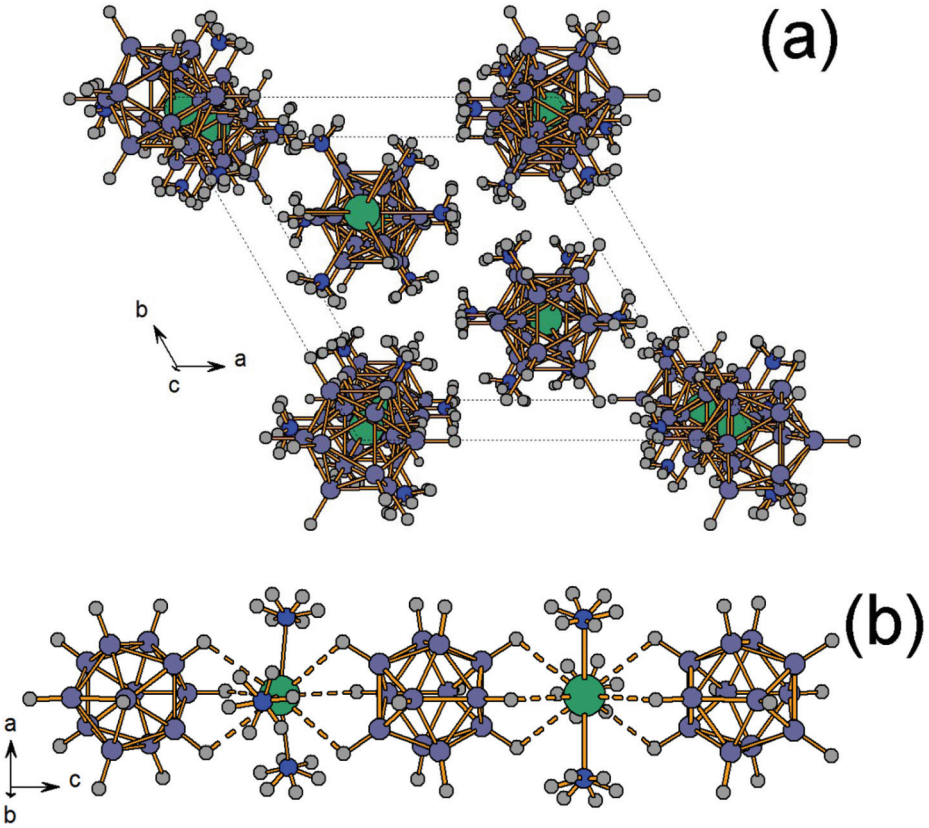

Fig. 5 Crystal structure of $CaB_{12}H_{12}{\cdot}3NH_3$ showing (a) the unit cell in the *ab*-plane and (b) the one dimensional chains observed in the *ac*-plane. Ca-Atoms have 9-fold coordination with six H-atoms (dashed) and three NH_3 molecules. Owing to the elevated temperature, the H-positions of NH_3 are not fixed. Atoms are shown as colored spheres: Ca (olive), N (blue), B (blue-grey) and H (grey). More structural information is available in Tables 2 and S8, S9.†

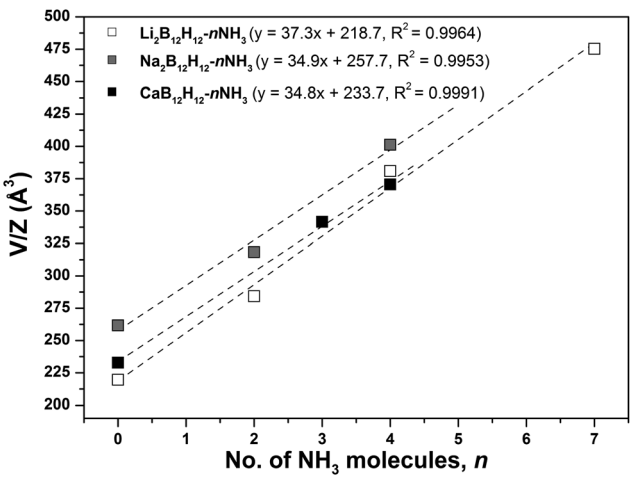

Fig. 6 Unit cell volumes (*V*) divided by the number of formula units (*Z*) plotted as a function of number of ammonia in the formula unit (*n*) are shown for $Li_2B_{12}H_{12}{\cdot}nNH_3$, *n* = 0, 2, 4 and 7, $Na_2B_{12}H_{12}{\cdot}nNH_3$, *n* = 0, 2 and 4, $CaB_{12}H_{12}{\cdot}nNH_3$, *n* = 0, 3 and 4. Linear fits are added as guides to the eye. Volumes of $Li_2B_{12}H_{12}$, $Na_2B_{12}H_{12}$, $CaB_{12}H_{12}$ and $Li_2B_{12}H_{12}{\cdot}7NH_3$ are extracted from previously reported structures.[8,20,49,53]

formed. From RT–75 °C diffraction from $Li_2B_{12}H_{12}{\cdot}7NH_3$ is observed by *in situ* SR-PXD but decreases in intensity from *T* = 60 °C, while Bragg peaks from $Li_2B_{12}H_{12}{\cdot}4NH_3$ appear and increase in intensity (Fig. 7b2). This is in agreement with TGA-DSC-MS data (Fig. 8) where a mass loss of 16.8 wt% NH_3 between *T* = 60–110 °C is observed (calculated mass loss for three NH_3 molecules is 18.6 wt%). The lower mass loss is discussed later. By *in situ* SR-PXD, thermal expansion of $Li_2B_{12}H_{12}{\cdot}4NH_3$ is observed from $T \approx 150$ °C, where several peaks shift *ca.* 0.1° towards lower 2θ values (higher *d*-spacing), indicated with dashed lines in Fig. 7b3. At *T* = 190 °C Bragg peaks from $Li_2B_{12}H_{12}{\cdot}2NH_3$ are observed by *in situ* SR-PXD, which correlates well with TGA-DSC-MS data, showing two endothermic events and a mass loss of 11.7 wt% from two NH_3 molecules (calc. mass loss 12.4 wt%) in the temperature range 160–225 °C.

The $Li_2B_{12}H_{12}{\cdot}7NH_3$ sample was also studied using TPPA, providing visual inspection of the thermal events (Fig. S9†). The pellet visibly shrinks in two steps from 55–115 °C and from 145–185 °C (Fig. S9a–c†), which correlates well with the first two NH_3 releases observed with *in situ* SR-PXD and TGA-DSC-MS. The sample melts at $T \approx 190$ °C and transforms to a transparent liquid containing a white, cloudy suspension

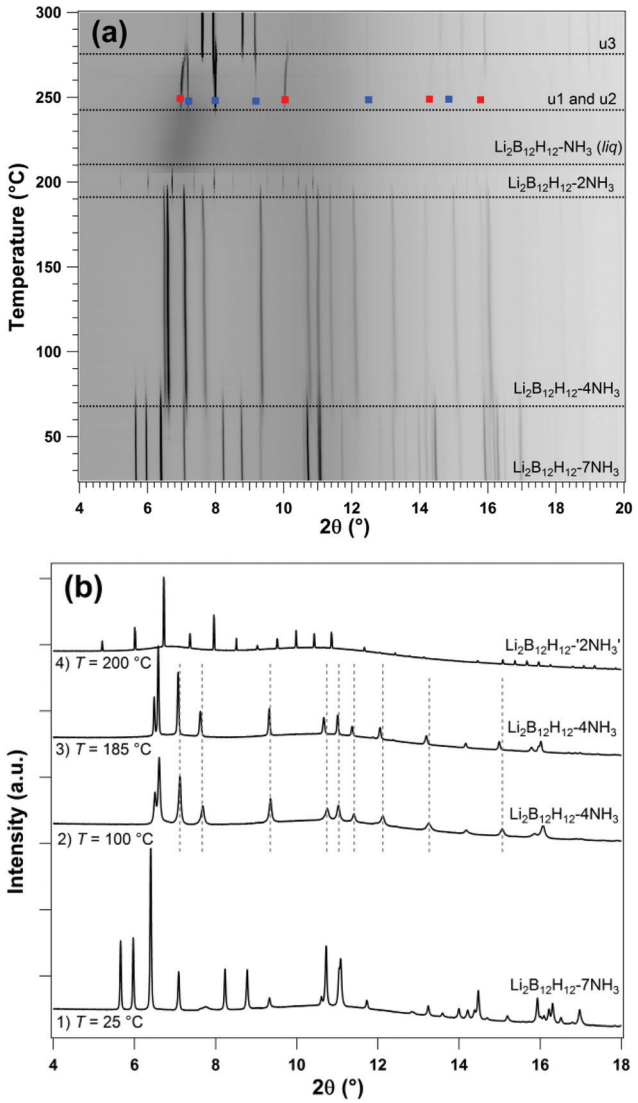

Fig. 7 (a) *In situ* SR-PXD of $Li_2B_{12}H_{12}$·$7NH_3$ in the temperature range RT–300 °C ($\Delta T/\Delta t$ = 5 °C min^{-1}), p(Ar) = 1 bar, λ = 0.7750 Å. (b) Selected diffraction patterns from (a) at (1) T = 25 °C, (2) T = 100 °C, (3) T = 185 °C and (4) T = 200 °C. Symbols: **u1** (red square), **u2** (blue square).

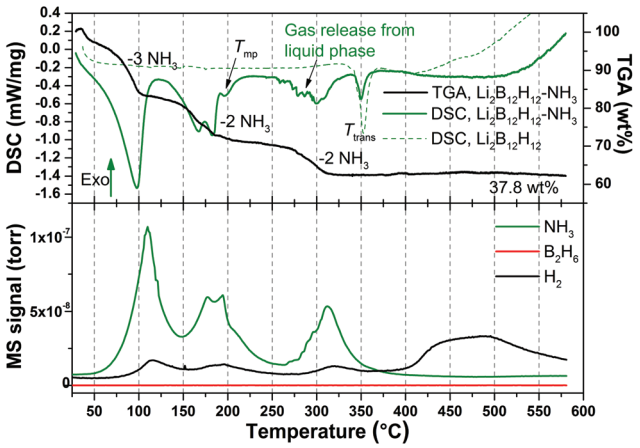

Fig. 8 TGA-DSC-MS of $Li_2B_{12}H_{12}$·$7NH_3$ and DSC of anhydrous $Li_2B_{12}H_{12}$ (dashed) in the temperature range RT–585 °C ($\Delta T/\Delta t$ = 5 °C min^{-1}, Ar-flow of 50 mL min^{-1}).

(Fig. S9d†). The melting is also observed by DSC at $T \approx 190$ °C and at 210 °C by *in situ* SR-PXD, where only a broad hump at $2\theta = 6.5°$ is observed. Upon further heating, TPPA data reveal drying of the droplet, and slowly it increases in size. This 'drying-process' is supported by *in situ* SR-PXD, where diffraction reappears at T = 240 °C. Here, there are two unknown compounds (denoted **u1** and **u2**), where **u1** shifts gradually towards higher 2θ, indicating a decreasing unit cell volume, which may support the continuous NH_3 release as observed in TGA-DSC-MS in this temperature range (250–350 °C). It was not possible to obtain a unit cell from indexing of either **u1** or **u2**.

Another set of diffraction peaks from an unknown compound (denoted **u3**) is observed at 275 °C that continue until 300 °C, when the *in situ* SR-PXD experiment was stopped. By TGA-DSC-MS, a mass loss of 9.2 wt% NH_3 is detected in the temperature range 260–325 °C, indicating the loss of 1–2 NH_3 molecules (calc. mass loss 6.2–12.4 wt%). Furthermore, the order–disorder transition and decomposition of $Li_2B_{12}H_{12}$ is observed in TGA-DSC at T = 350 and 410 °C which coincides with anhydrous $Li_2B_{12}H_{12}$ as shown with the dashed line in the DSC data.[19] The melting of the sample may explain the irregular DSC signal observed from 200–325 °C since the TPPA data indicate that NH_3 is released in a drying process where pure or partly ammoniated $Li_2B_{12}H_{12}$ is left as a brittle, powdery crust.

The observation of a liquid intermediate has been reported for $LiBH_4$ with NH_3.[54] $LiBH_4$ can form three ammoniates under varying NH_3 partial pressures at RT, *i.e.* $LiBH_4$·xNH_3 (x = 1, 2, 3). $LiBH_4$·$2NH_3$ is liquid, whereas $LiBH_4$·NH_3 and $LiBH_4$·$3NH_3$ are solid.[54] The TGA-DSC-MS data of $Li_2B_{12}H_{12}$·$7NH_3$ suggest that the liquid compound may have a composition near $Li_2B_{12}H_{12}$·$n$$NH_3$ ($1 < n < 2$).

Although the initial PXD data only show diffraction from $Li_2B_{12}H_{12}$·$7NH_3$, the total observed mass loss by TGA, 37.8 wt%, is less than the calculated mass loss for the release of 7 NH_3 molecules, 43.3 wt%. Surprisingly, the NH_3-release between 260 and 325 °C is not observed in a previous report of $Li_2B_{12}H_{12}$·$7NH_3$, where release of 43.3 wt% NH_3 below 200 °C was realized.[20] However, the present DSC events observed below 200 °C occur at temperatures similar to the previous report. Even though the starting material is similar, the samples clearly behave differently, perhaps owing to differences in the experimental setup or synthesis. The low mass loss may be a result of the sample not being fully ammoniated, even though $Li_2B_{12}H_{12}$·$7NH_3$ was the only observed compound, or the sample contains an amorphous impurity, although no indication hereof is currently identified.

Thermal decomposition of $Na_2B_{12}H_{12}$·$4NH_3$. The *in situ* SR-PXD data in Fig. 9 present the thermal decomposition of $Na_2B_{12}H_{12}$·$4NH_3$. A diffractogram obtained at RT before the

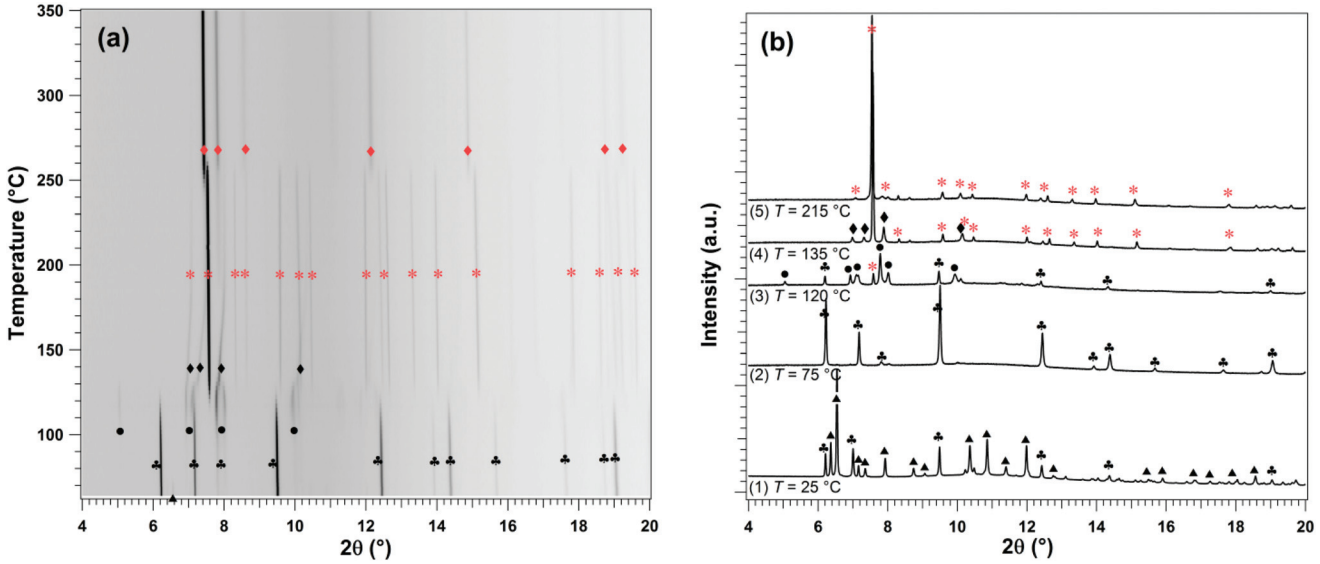

Fig. 9 (a) *In situ* SR-PXD of $Na_2B_{12}H_{12}{\cdot}4NH_3$ in the temperature range 65–350 °C ($\Delta T/\Delta t$ = 5 °C min^{-1}), p(Ar) = 1 bar, λ = 0.7750 Å. (b) Selected diffraction patterns from the *in situ* data, (1) T = 25 °C, (2) T = 75 °C, (3) T = 120 °C, (4) T = 135 °C, (5) T = 215 °C. Symbols: $Na_2B_{12}H_{12}{\cdot}4NH_3$ (black triangles), $Na_2B_{12}H_{12}{\cdot}2NH_3$ (black spades), **u4** (black circles), **u5** (black diamonds), $Na_2B_{12}H_{12}$ (red asterisk) and *HT*-$Na_2B_{12}H_{12}$ (red diamonds).

experiment, shows a mixture of both $Na_2B_{12}H_{12}{\cdot}4NH_3$ and $Na_2B_{12}H_{12}{\cdot}2NH_3$, indicating some ammonia had been released prior to the experiment (Fig. 9b1). Diffracted intensity of $Na_2B_{12}H_{12}{\cdot}4NH_3$ disappears at ~70 °C and diffracted intensity from $Na_2B_{12}H_{12}{\cdot}2NH_3$ begins to disappear at T = 100 °C, but is observed until 125 °C (Fig. 9b2). At this temperature a third compound (denoted **u4**) appears which is observed until ~135 °C (Fig. 9b3). Following this, diffraction from $Na_2B_{12}H_{12}$ is observed together with a few peaks from another unknown compound (denoted **u5**) that gradually shifts towards higher 2θ values in the temperature range 135–190 °C (Fig. 9b4). This indicates a decrease in unit cell volume, likely as a consequence of NH_3 release. The suggested composition of **u4** may be $Na_2B_{12}H_{12}{\cdot}NH_3$ and **u5** may be $Na_2B_{12}H_{12}{\cdot}0.5NH_3$ or $Na_2B_{12}H_{12}$ with 1–2 interstitial NH_3 molecules, however the composition could not be structurally determined. At T > 200 °C, $Na_2B_{12}H_{12}$ is the only observed compound and the high-temperature order–disorder phase transition of $Na_2B_{12}H_{12}$ is observed at 260 °C (Fig. 9b5). This indicates all NH_3 is released below 200 °C.

The thermal analysis of $Na_2B_{12}H_{12}{\cdot}4NH_3$ (Fig. 10) correlates well with the *in situ* SR-PXD data as three endothermic events are observed at T = 80, 125 and 140 °C. The phase transition of $Na_2B_{12}H_{12}$ occurs at 268 °C and the sample starts to decompose at an onset temperature of $T \approx$ 400 °C, in agreement with the behavior of pure $Na_2B_{12}H_{12}$ (shown as dashed lines in Fig. 10). The total observed mass loss is 19.0 wt%, but the calculated ammonia content of $Na_2B_{12}H_{12}{\cdot}4NH_3$ is 26.6 wt% NH_3. As shown in Fig. 9a both $Na_2B_{12}H_{12}{\cdot}4NH_3$ and $Na_2B_{12}H_{12}{\cdot}2NH_3$ are observed, indicating that some $Na_2B_{12}H_{12}{\cdot}4NH_3$ converts to $Na_2B_{12}H_{12}{\cdot}2NH_3$ at room temperature after synthesis. Hence, $Na_2B_{12}H_{12}{\cdot}4NH_3$ may have limited stability at RT.

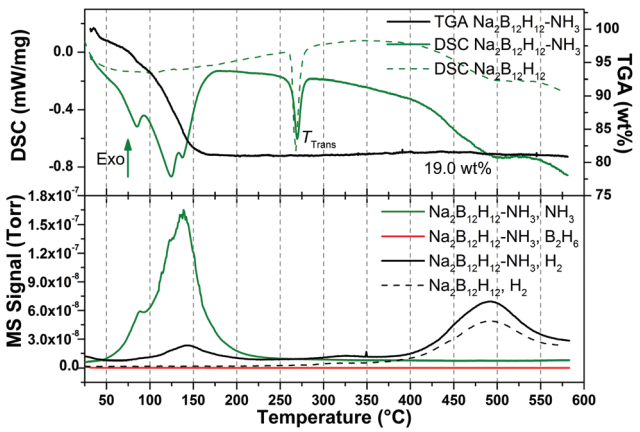

Fig. 10 TGA-DSC-MS of $Na_2B_{12}H_{12}{\cdot}4NH_3$ and DSC of anhydrous $Na_2B_{12}H_{12}$ (dashed) from RT–585 °C ($\Delta T/\Delta t$ = 5 °C min^{-1} with an Ar-flow of 50 mL min^{-1}).

In the TPPA measurement of $Na_2B_{12}H_{12}{\cdot}4NH_3$, shrinkage of the pellet was observed from 60–100 °C and 112–150 °C (Fig. S10†) agreeing well with the observations from thermal analysis and the *in situ* SR-PXD data. Another visual change occurs above the phase transition of $Na_2B_{12}H_{12}$ at 270 °C, where the pellet slowly increases in volume until the measurement is stopped at 350 °C, possibly underlining the higher volume of the disordered high-temperature polymorph of $Na_2B_{12}H_{12}$.[55]

Thermal decomposition of $CaB_{12}H_{12}{\cdot}6NH_3$. Thermal analysis of sample $CaB_{12}H_{12}{\cdot}6NH_3$, presented in Fig. 11, shows four thermal events where NH_3 is released, followed by decomposition of $CaB_{12}H_{12}$ starting at T = 350 °C with H_2 release. The TGA-DSC-MS data indicate that the four NH_3-release events occur as follows: two NH_3 molecules are

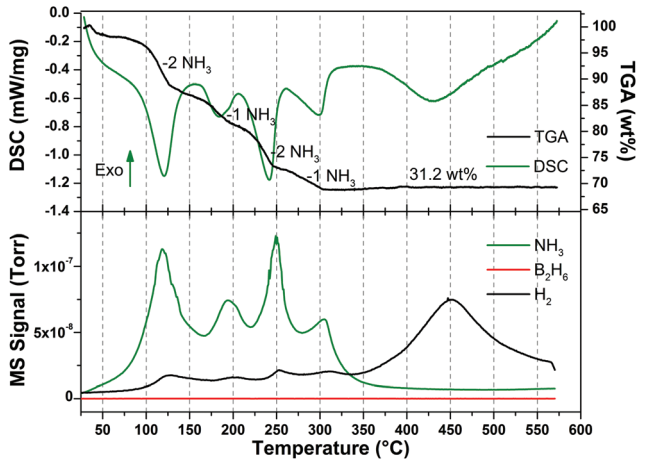

Fig. 11 TGA-DSC-MS of $CaB_{12}H_{12}{\cdot}6NH_3$ in the temperature range RT–585 °C ($\Delta T/\Delta t$ = 5 °C min^{-1}, Ar-flow = 50 mL min^{-1}).

released at T = 120 °C, one NH_3 molecule is released at T = 200 °C, two NH_3 molecules are released at T = 250 °C, and one NH_3 molecule is released at T = 310 °C. The TGA data reveal a total mass loss of 31.2 wt%, which is lower than the calculated 36.0 wt% NH_3 of $CaB_{12}H_{12}{\cdot}6NH_3$. TPPA shows that the pellet decreases in volume in multiple steps corresponding to the NH_3 release, observed at temperatures equal to the TGA-DSC-MS data (Fig. S11†).

The *in situ* SR-PXD data are presented in Fig. 12, where the decomposition of $CaB_{12}H_{12}{\cdot}6NH_3$ reveals five different unknown structures. The observed structural changes fit well with the thermal analysis. It was not possible to index or solve most of the structures owing to peak overlap and low crystallinity, however the structural solutions and composition of $CaB_{12}H_{12}{\cdot}4NH_3$ (observed between 90–190 °C) and $CaB_{12}H_{12}{\cdot}3NH_3$ (190–260 °C) agree well with the thermal analysis where the DSC signal and TGA mass loss indicate the release of ~3 NH_3 molecules from RT–200 °C. By combining TGA and *in situ* SR-PXD data, the unknown structures may be assigned as: $CaB_{12}H_{12}{\cdot}$'$6NH_3$' (RT–70 °C), $CaB_{12}H_{12}{\cdot}$'$5NH_3$' (70–90 °C), $CaB_{12}H_{12}{\cdot}4NH_3$ (90–190 °C), $CaB_{12}H_{12}{\cdot}3NH_3$ (190–260 °C), and $CaB_{12}H_{12}{\cdot}$'NH_3' (260–>275 °C). Another *in situ* SR-PXD experiment was conducted at Maxlab (beamline I711), where the sample was heated to 450 °C. Here the formation of $CaB_{12}H_{12}$ and subsequent decomposition was observed at 300 and 350 °C, in agreement with the thermal analysis (Fig. S12†). Thus, the sample does not decompose until all NH_3 has been released, similar to what was observed in ammoniated $Li_2B_{12}H_{12}$ and $Na_2B_{12}H_{12}$.

Ammonia release and uptake

The reversible NH_3 release and uptake for $Li_2B_{12}H_{12}{\cdot}7NH_3$ has been reported previously, where a sample of $Li_2B_{12}H_{12}$ remains unchanged after 10 cycles, indicating excellent reversibility of NH_3 release and uptake.[20] Here the high thermal stability of metal dodecahydro-*closo*-dodecaborane is an advantage, as it allows the release and uptake of NH_3 at moderate temperatures

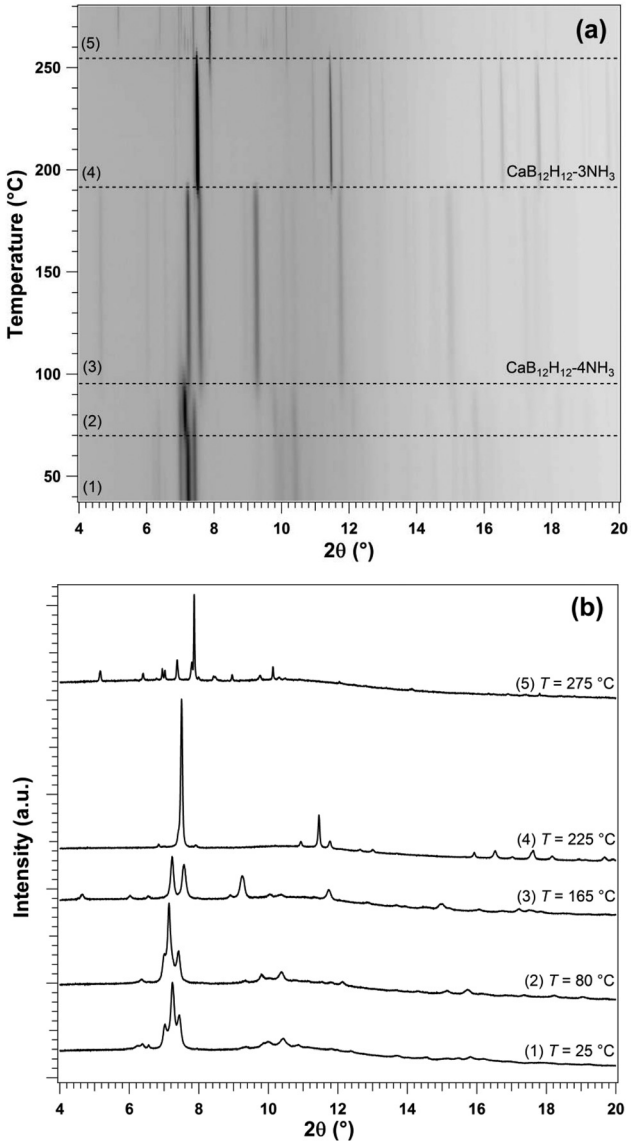

Fig. 12 (a) *In situ* SR-PXD of $CaB_{12}H_{12}{\cdot}6NH_3$ in the temperature range RT–275 °C ($\Delta T/\Delta t$ = 5 °C min^{-1}), p(Ar) = 1 bar, λ = 0.7750 Å. (b) Selected diffraction pattern from (a): (1) T = 25 °C, (2) T = 80 °C (3) T = 165 °C, (4) T = 225 °C, (5) T = 275 °C.

without altering or decomposing the metal dodecahydro-*closo*-dodecaborane. For $Na_2B_{12}H_{12}$ and $CaB_{12}H_{12}$, the reversible release and uptake of NH_3 was demonstrated by powder X-ray diffraction as presented in Fig. 13 and 14. In both cases, NH_3 is absorbed at RT and released at 250 and 300 °C under dynamic vacuum for $Na_2B_{12}H_{12}$ and $CaB_{12}H_{12}$, respectively. Both $Na_2B_{12}H_{12}$ and $CaB_{12}H_{12}$ show good reversibility over two NH_3 release and uptake cycles.

Discussion

The thermal decomposition of ammine $M_xB_{12}H_{12}$ (M = Li, Na, Ca) shows that NH_3 was released from all samples in multiple

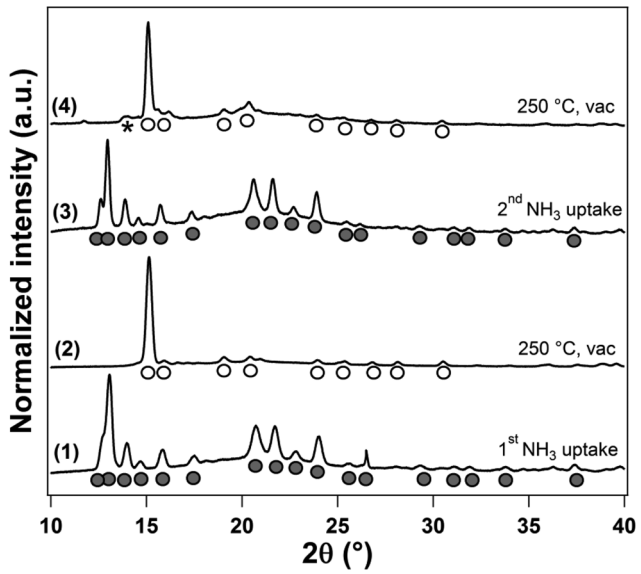

Fig. 13 Diffractograms obtained after NH_3 release and uptake in $Na_2B_{12}H_{12}{\cdot}4NH_3$ (λ = 1.5418 Å). The diffractograms show (1) as synthesized $Na_2B_{12}H_{12}{\cdot}4NH_3$, (2) first desorption at 250 °C, vac., (3) second NH_3 uptake in $Na_2B_{12}H_{12}$, and (4) second desorption at 250 °C, vac. Symbols: $Na_2B_{12}H_{12}{\cdot}4NH_3$ (grey circle), $Na_2B_{12}H_{12}$ (white circle) and unknown (black asterisk).

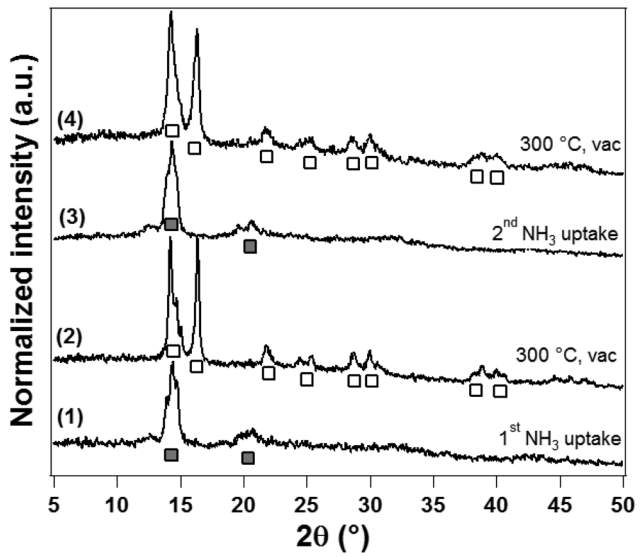

Fig. 14 Diffractograms obtained after NH_3 release and uptake in $CaB_{12}H_{12}{\cdot}6NH_3$ (λ = 1.5418 Å). The diffractograms show (1) as-synthesized $CaB_{12}H_{12}{\cdot}6NH_3$ (2) first desorption at 300 °C, vac. (3) second NH_3 uptake, and (4) second desorption at 300 °C, vac. Symbols: $CaB_{12}H_{12}{\cdot}6NH_3$ (grey square) and $CaB_{12}H_{12}$ (white square).

steps, giving rise to interesting structural changes observed by *in situ* synchrotron radiation X-ray diffraction. The thermal decomposition of $Li_2B_{12}H_{12}{\cdot}7NH_3$ is complex with several intermediate ammine metal dodecahydro-*closo*-dodecaboranes, and two are structurally identified. At *ca.* 190 to 240 °C, the sample is molten and after recrystallization several unknown compounds are observed. For $Na_2B_{12}H_{12}{\cdot}4NH_3$ the release of ammonia occurs in three steps and the intermediate compound $Na_2B_{12}H_{12}{\cdot}2NH_3$ was solved. $CaB_{12}H_{12}$ releases *ca.* six ammonia molecules in four steps and two intermediate compounds are determined as $CaB_{12}H_{12}{\cdot}4NH_3$ and $CaB_{12}H_{12}{\cdot}3NH_3$.

The samples only release NH_3 and the decomposition temperature of the metal dodecahydro-*closo*-dodecaborane is unaltered compared to pristine metal dodecahydro-*closo*-dodecaborane. It should be noted that minor release of H_2 is detected simultaneously with NH_3 in the MS of all three samples. A fragmentation overlap in the MS between NH_3 and H_2 is typically not expected and it is believed to be an artifact from the experimental setup. A part of the coupling line between TGA-DSC and MS is made of plastic and contain a filter to prevent powder from entering the MS capillary. It is possible this filter was dirty and, when exposed to ammonia, hydrogen from a side reaction could be carried trough. Nevertheless, the observation of the pure $M_xB_{12}H_{12}$ compounds by *in situ* SR-PXD, and the fact that NH_3 is reversible cycled, allows us to conclude that no decomposition occurs when NH_3 is released. Furthermore, no formation of stable B–N compounds is observed in this investigation, otherwise reported for some ammine metal borohydrides, *e.g.* $Mn(BH_4)_2{\cdot}6NH_3$ in an exothermic reaction possibly *via* dihydrogen bonds between BH_4^- and NH_3 ($H^{\delta-}\cdots^{\delta+}H$).[24] Other more stable metal borohydrides release ammonia without reaction, and may store ammonia reversibly, *e.g.* $M(BH_4)_2$, M = Ca or Sr.[1,51,56] The high thermal stability of the metal dodecahydro-*closo*-dodecaboranes makes them suitable for NH_3 storage at low to moderate temperatures, and the reversibility is demonstrated for ammine $Na_2B_{12}H_{12}$ and $CaB_{12}H_{12}$, and reported previously for ammine $Li_2B_{12}H_{12}$.[20] The reported temperatures for NH_3 release in $Li_2B_{12}H_{12}{\cdot}7NH_3$ (release of 43.3 wt% NH_3 at 200 °C) differ significantly from the ammonia release observed by *in situ* SR-PXD, TGA-DSC-MS and TPPA in the present study (release of 37.4 wt% NH_3 below 350 °C) and these results are reproducible for multiple samples. It remains unclear why such large differences to the previous report are observed, since deviations of this magnitude are not typically ascribed to only experimental differences or synthesis conditions.

The gravimetric NH_3 density may limit the potential NH_3 storage in the light metal dodecahydro-*closo*-dodecaboranes studied here, since the $[B_{12}H_{12}]^{2-}$ anion is heavy compared to chloride. For instance, $MgCl_2{\cdot}6NH_3$ absorbs ammonia at RT and releases a total of 51.77 wt% ammonia in three steps at temperatures comparable to the metal dodecahydro-*closo*-dodecaboranes (150 to 325 °C).[30] Nevertheless, the total hydrogen content of the ammine metal dodecahydro-*closo*-dodecaboranes is high (Tables 2 and 3), but only hydrogen indirectly stored as NH_3 is reversibly accessible. For comparison, the hydrogen content of selected ammine metal chlorides is listed together with the studied ammine metal dodecahydro-*closo*-dodecaboranes in Table 3.

Table 3 The ammonia and hydrogen content of selected ammine metal chlorides and dodecahydro-*closo*-dodecaboranes[30]

Compound	M (g mol^{-1})	NH_3 content (wt%)	H content from NH_3 [a] (wt%)	Total H content (wt%)	Ref.
$CaCl_2{\cdot}8NH_3$	247.23	41.33	9.78	9.78	30
$MgCl_2{\cdot}6NH_3$	197.40	51.77	9.19	9.19	30
$Li_2B_{12}H_{12}{\cdot}7NH_3$	274.93	43.36	7.70	12.10	20 + This work
$Na_2B_{12}H_{12}{\cdot}4NH_3$	255.93	26.62	4.73	9.45	This work
$CaB_{12}H_{12}{\cdot}6NH_3$	284.09	35.97	6.39	10.64	This work

[a] Only hydrogen originating from NH_3 is considered.

Conclusions

This investigation reveals the synthesis and complex ammonia release reactions from $Li_2B_{12}H_{12}{\cdot}7NH_3$, $Na_2B_{12}H_{12}{\cdot}4NH_3$, and $CaB_{12}H_{12}{\cdot}6NH_3$. The thermal decomposition is investigated using a range of complementary techniques, *in situ* time-resolved synchrotron radiation powder X-ray diffraction (*in situ* SR-PXD), thermal analysis (TGA-DSC-MS), Fourier transformed infrared spectroscopy (FTIR), and temperature programmed photographic analysis (TPPA). The ammonia release reactions reveal fifteen new compounds, where six of those are structurally characterized. This work shows that ammine metal dodecahydro-*closo*-dodecaboranes have ammonia storage density and properties comparable to similar metal halides, mainly assigned to the high thermal stability of large dodecahydro-*closo*-dodecaborane anions. Furthermore, ammonia is stored reversibly and may be considered as indirect hydrogen storage. This work provides deeper insight into the structural, physical, and chemical properties related to thermal decomposition and possible ammonia and hydrogen storage of metal dodecahydro-*closo*-dodecaborane-based materials.

Acknowledgements

The work was supported by the Innovation Fund Denmark (project HyFill-Fast), the Danish Research Council for Nature and Universe (Danscatt), Danish council for independent research (HyNanoBorN, DFF-4181-00462), the European Marie Curie Actions under ECOSTORE grant agreement no. 607040, the Danish National Research Foundation, and Center for Materials Crystallography (DNRF93). We are grateful to the Carlsberg Foundation. This work was partly supported by the Fonds de la Recherche Scientifique FNRS. We are grateful for the allocated beam time at Petra III, MAX-lab and the Materials Science Beamline X04SA, SLS/PSI (proposal number 20140366) and Dr Nicola Casati and Dr Voraksmy Ban for the help.

References

1 M. Paskevicius, L. H. Jepsen, P. Schouwink, R. Černý, D. B. Ravnsbæk, Y. Filinchuk, M. Dornheim, F. Besenbacher and T. R. Jensen, *Chem. Soc. Rev.*, 2017, **46**, 1565–1634.
2 L. H. Rude, T. K. Nielsen, D. B. Ravnsbæk, U. Bösenberg, M. B. Ley, B. Richter, L. M. Arnbjerg, M. Dornheim, Y. Filinchuk, F. Besenbacher and T. R. Jensen, *Phys. Status Solidi A*, 2011, **208**, 1754–1773.
3 M. Felderhoff, C. Weidenthaler, R. von Helmolt and U. Eberle, *Phys. Chem. Chem. Phys.*, 2007, **9**, 2643–2653.
4 S. Orimo, Y. Nakamori, J. R. Eliseo, A. Züttel and C. M. Jensen, *Chem. Rev.*, 2007, **107**, 4111–4132.
5 B. R. S. Hansen, M. Paskevicius, H.-W. Li, E. Akiba and T. R. Jensen, *Coord. Chem. Rev.*, 2016, **323**, 60–70.
6 B. R. S. Hansen, D. B. Ravnsbæk, D. Reed, D. Book, C. Gundlach, J. Skibsted and T. R. Jensen, *J. Phys. Chem. C*, 2013, **117**, 7423–7432.
7 B. R. S. Hansen, D. B. Ravnsbæk, J. Skibsted and T. R. Jensen, *Phys. Chem. Chem. Phys.*, 2014, **16**, 8970–8980.
8 J.-H. Her, M. Yousufuddin, W. Zhou, S. S. Jalisatgi, J. G. Kulleck, J. A. Zan, S.-J. Hwang, R. C. Bowman and T. J. Udovic, *Inorg. Chem.*, 2008, **47**, 9757–9759.
9 S.-J. Hwang, R. C. Bowman, J. W. Reiter, J. Rijssenbeek, G. L. Soloveichik, J.-C. Zhao, H. Kabbour and C. C. Ahn, *J. Phys. Chem. C*, 2008, **112**, 3164–3169.
10 H.-W. Li, K. Miwa, N. Ohba, T. Fujita, T. Sato, Y. Yan, S. Towata, M. W. Chen and S. Orimo, *Nanotechnology*, 2009, **20**, 204013.
11 Y. Yan, A. Remhof, S.-J. Hwang, H.-W. Li, P. Mauron, S. Orimo and A. Züttel, *Phys. Chem. Chem. Phys.*, 2012, **14**, 6514–6519.
12 M. F. Hawthorne, *Mol. Med. Today*, 1998, **4**, 174–181.
13 C. Salt, A. J. Lennox, M. Takagaki, J. A. Maguire and N. S. Hosmane, *Russ. Chem. Bull.*, 2004, **53**, 1871–1888.
14 T. J. Udovic, M. Matsuo, A. Unemoto, N. Verdal, V. Stavila, A. V. Skripov, J. J. Rush, H. Takamura and S. Orimo, *Chem. Commun.*, 2014, **50**, 3750–3752.
15 L. He, H.-W. Li, H. Nakajima, N. Tumanov, Y. Filinchuk, S.-J. Hwang, M. Sharma, H. Hagemann and E. Akiba, *Chem. Mater.*, 2015, **27**, 5483–5486.
16 Y. Sadikin, M. Brighi, P. Schouwink and R. Černý, *Adv. Energy Mater.*, 2015, **5**, DOI: 10.1002/aenm.201501016.
17 M. Paskevicius, B. R. S. Hansen, M. Jørgensen, B. Richter and T. R. Jensen, *Nat. Commun.*, 2017, **8**, 15136.
18 F. Cheng and F. Jäkle, *Polym. Chem.*, 2011, **2**, 2122–2132.
19 M. P. Pitt, M. Paskevicius, D. H. Brown, D. A. Sheppard and C. E. Buckley, *J. Am. Chem. Soc.*, 2013, **135**, 6930–6941.

20 Z. Huang, J. Gallucci, X. Chen, T. Yisgedu, H. K. Lingam, S. G. Shore and J.-C. Zhao, *J. Mater. Chem.*, 2010, **20**, 2743–2745.
21 D. Miura and T. Tezuka, *Energy*, 2014, **68**, 428–436.
22 A. Klerke, C. H. Christensen, J. K. Nørskov and T. Vegge, *J. Mater. Chem.*, 2008, **18**, 2304–2310.
23 R. Z. Sørensen, J. S. Hummelshøj, A. Klerke, J. B. Reves, T. Vegge, J. K. Nørskov and C. H. Christensen, *J. Am. Chem. Soc.*, 2008, **130**, 8660–8668.
24 L. H. Jepsen, M. B. Ley, Y. Filinchuk, F. Besenbacher and T. R. Jensen, *ChemSusChem*, 2015, **8**, 1452–1463.
25 F. Kraus, M. Panda, T. Müller and B. Albert, *Inorg. Chem.*, 2013, **52**, 4692–4699.
26 W. I. F. David, J. W. Makepeace, S. K. Callear, H. M. A. Hunter, J. D. Taylor, T. J. Wood and M. O. Jones, *J. Am. Chem. Soc.*, 2014, **136**, 13082–13085.
27 L. H. Jepsen, P. Wang, G. Wu, Z. Xiong, F. Besenbacher, P. Chen and T. R. Jensen, *Phys. Chem. Chem. Phys.*, 2016, **18**, 25257–25264.
28 A. Wojcik, H. Middleton, I. Damopoulos and J. Van herle, *J. Power Sources*, 2003, **118**, 342–348.
29 T. D. Elmøe, R. Z. Sørensen, U. Quaade, C. H. Christensen, J. K. Nørskov and T. Johannessen, *Chem. Eng. Sci.*, 2006, **61**, 2618–2625.
30 C. H. Christensen, R. Z. Sørensen, T. Johannessen, U. J. Quaade, K. Honkala, T. D. Elmøe, R. Køhler and J. K. Nørskov, *J. Mater. Chem.*, 2005, **15**, 4106–4108.
31 Y. Liu, R. Ma, R. Luo, K. Luo, M. Gao and H. Pan, *Mater. Trans.*, 2011, **52**, 627–634.
32 L. Gao, Y. H. Guo, Q. Li and X. B. Yu, *J. Phys. Chem. C*, 2010, **114**, 9534–9540.
33 M. Paskevicius, M. P. Pitt, D. H. Brown, D. A. Sheppard, S. Chumphongphan and C. E. Buckley, *Phys. Chem. Chem. Phys.*, 2013, **15**, 15825–15828.
34 Y. Cerenius, K. Ståhl, L. A. Svensson, T. Ursby, Å. Oskarsson, J. Albertsson and A. Liljas, *J. Synchrotron Radiat.*, 2000, **7**, 203–208.
35 T. R. Jensen, T. K. Nielsen, Y. Filinchuk, J.-E. Jørgensen, Y. Cerenius, E. M. Gray and C. J. Webb, *J. Appl. Crystallogr.*, 2010, **43**, 1456–1463.
36 K. T. Møller, B. R. S. Hansen, A.-C. Dippel, J.-E. Jørgensen and T. R. Jensen, *Z. Anorg. Allg. Chem.*, 2014, **640**, 3029–3043.
37 B. R. S. Hansen, K. T. Møller, M. Paskevicius, A.-C. Dippel, P. Walter, C. J. Webb, C. Pistidda, N. Bergemann, M. Dornheim, T. Klassen, J.-E. Jørgensen and T. R. Jensen, *J. Appl. Crystallogr.*, 2015, **48**, 1234–1241.
38 A.-C. Dippel, N. Bindzus, D. Saha, J. T. Delitz, H.-P. Liermann, N. Wahlberg, J. Becker, E. D. Bøjesen and B. Brummerstedt Iversen, *Z. Anorg. Allg. Chem.*, 2014, **640**, 3094–3099.
39 C. Pistidda, A. Santoru, S. Garroni, N. Bergemann, A. Rzeszutek, C. Horstmann, D. Thomas, T. Klassen and M. Dornheim, *J. Phys. Chem. C*, 2015, **119**, 934–943.
40 A. P. Hammersley, S. O. Svensson, M. Hanfland, A. N. Fitch and D. Hausermann, *High Pressure Res.*, 1996, **14**, 235–248.
41 V. Favre-Nicolin and R. Černý, *J. Appl. Crystallogr.*, 2002, **35**, 734–743.
42 J. Rodríguez-Carvajal, *Physica B*, 1993, **192**, 55–69.
43 M. Paskevicius, M. B. Ley, D. A. Sheppard, T. R. Jensen and C. E. Buckley, *Phys. Chem. Chem. Phys.*, 2013, **15**, 19774–19789.
44 E. L. Muetterties, R. E. Merrifield, H. C. Miller, W. H. Knoth and J. R. Downing, *J. Am. Chem. Soc.*, 1962, **84**, 2506–2508.
45 M. Sharma, D. Sethio, V. D'Anna and H. Hagemann, *Int. J. Hydrogen Energy*, 2015, **40**, 12721–12726.
46 D. Sethio, L. M. Lawson Daku and H. Hagemann, *Int. J. Hydrogen Energy*, 2016, **41**, 6814–6824.
47 I. Tiritiris, J. Weidlein and T. Schleid, *Z. Naturforsch., B: Chem. Sci.*, 2005, **60**, 627–639.
48 S. Westman, P.-E. Werner, T. Schuler and W. Raldow, *Acta Chem., Scand. Ser. A*, 1981, **35**, 467–472.
49 V. Stavila, J.-H. Her, W. Zhou, S.-J. Hwang, C. Kim, L. A. M. Ottley and T. J. Udovic, *J. Solid State Chem.*, 2010, **183**, 1133–1140.
50 I. Olovsson and D. H. Templeton, *Acta Crystallogr.*, 1959, **12**, 832–836.
51 L. H. Jepsen, Y.-S. Lee, R. Černý, R. S. Sarusie, Y. W. Cho, F. Besenbacher and T. R. Jensen, *ChemSusChem*, 2015, **8**, 3472–3482.
52 L. H. Jepsen, M. B. Ley, R. Černý, Y.-S. Lee, Y. W. Cho, D. Ravnsbæk, F. Besenbacher, J. Skibsted and T. R. Jensen, *Inorg. Chem.*, 2015, **54**, 7402–7414.
53 J.-H. Her, W. Zhou, V. Stavila, C. M. Brown and T. J. Udovic, *J. Phys. Chem. C*, 2009, **113**, 11187–11189.
54 Y. Guo, G. Xia, Y. Zhu, L. Gao and X. Yu, *Chem. Commun.*, 2010, **46**, 2599–2601.
55 N. Verdal, J.-H. Her, V. Stavila, A. V. Soloninin, O. A. Babanova, A. V. Skripov, T. J. Udovic and J. J. Rush, *J. Solid State Chem.*, 2014, **212**, 81–91.
56 L. H. Jepsen, M. B. Ley, Y.-S. Lee, Y. W. Cho, M. Dornheim, J. O. Jensen, Y. Filinchuk, J. E. Jørgensen, F. Besenbacher and T. R. Jensen, *Mater. Today*, 2014, **17**, 129–135.